Time-Reversed Energy Sourced Through Localized Antennae

by

Gemstone Team TESLA

Submitted to the Department of Physics
in partial fulfillment of the requirements for the degree of

Gemstone Honors Program

at the

UNIVERSITY OF MARYLAND, COLLEGE PARK

May 2016

Author . . . .
Department of Physics
April 15, 2016

Certified by. . . . .
Steven Anlage
Professor
Thesis Supervisor

Accepted by . . . .
Frank Coale
Director, Gemstone Program

Time-Reversed Energy Sourced Through Localized Antennae

by

Gemstone Team TESLA

Abstract

We investigate the application of time reversed electromagnetic wave propagation to transmit energy to a moving target in a reverberant environment. âĂIJTime reversalâĂİ is a signal focusing method that exploits the time reversal invariance of the lossless wave equation to direct signals on a single point inside a complex scattering environment. In this work, we explore the properties of time-reversed microwave pulses in a low-loss raychaotic chamber. We measure the spatial profile of the collapsing wavefront around the target antenna, and demonstrate that time reversal can be used to transfer energy to a receiver in motion. We discuss the results of these experiments, and explore their implications for a wireless power transmission system based on time reversal

Thesis Supervisor: Steven Anlage
Title: Professor

Acknowledgments

Thank you mom.

Contents

List of Figures

List of Tables

Chapter 1

Introduction

In 1998, accessing the Internet required a clunky desktop computer and a dial-up subscription. When Apple integrated WiFi into its iBook computers under the brand name âĂIJAirPortâĂİ the following year, it forced other industry giants to compete and revolutionized wireless networking [2]. If not for the adoption of this technology along with the advent of wireless data-enabled and commercially available cell phones such as NokiaâĂŹs Communicator 9000 [1], cell phones would never have evolved to surpass their primary function as telephones and become the communication necessity they are today.

The ubiquity of WiFi and wireless communication revolutionized the way society interacts with the Internet. Suddenly, portable devices became powerful standalone devices rather than accessories to their desk-bound counterparts. Cell phones rivaled computers in necessity and ubiquity, and eclipsed their predecessors in terms of productivity. Coffee shops, airports, and hotels transformed from physical meeting places to universal hotspots, enabling the masses to bridge distances, connect instantly, and effectively trivialize time and space quite literally in the palms of their hands. This is the power of wireless technology.

So then, why does society continue to labor under the burden of wires? Having enjoyed rewards of another relatively nascent wireless technology, why do we hesitate to cut the cord?

Wireless power transfer (WPT)-enabled mobile devices have the potential to be a

disruptive technology on the consumer technology market. Investments in WPT have grown dramatically in the past decade, and more technologies have started integrating WPT into their systems at the consumer level.

The result is a growing number of WPT methods seeing practical application. These techniques can successfully power and charge a wide range of consumer products, from cell phones to cars. However, they still face significant disadvantages in transmission distance and efficiency. Most require line of sight to operate.

Gemstone Team TESLA proposes time-reversed electromagnetic wave propagation (to be abbreviated "time-reversal" or "TR" in this document) as a novel WPT method. In particular, TRâĂŹs ability to maintain connection even when line of sight is lost opens up a new range of possible applications. To support this proposal, the team has performed a number of exploratory experiments on the topic of TR applied to WPT. These experiments are concerned primarily with understanding the fundamental engineering realities that would be necessary to build a working TR WPT system.

In this paper, TESLA overviews the state of the art of both consumer wireless power transfer technologies and time reversal. Major innovations are outlined, as are current limitations. The teamâĂŹs experiments are then detailed individually. The purpose, methodology, and results for each experiment are explained. The results of each experiment and their significance are then discussed in the context of TR WPT. The results of the team as a whole are discussed in a similar way. Finally, the team makes suggestions for future research that could be made in this field, for the benefit of future researchers.

Chapter 2

Literature Review

In consideration of a solution to any problem, it is useful to consider the work that has already been done with regard to that problem. This step allows scientists to identify gaps in the current body of knowledge, build upon previous research, and generate questions for future investigation. By studying the efforts of their predecessors, researchers can gain a great deal of information about both the direction that their explorations should take and how to proceed in probing topics further. A review of current literature further serves to ensure that time is spent judiciously, and resources are not spent in answering the same question multiple times.

In this chapter, the efforts of several groups who have investigated the ability to send energy to electronic devices wirelessly will be considered. The idea of wireless power transmission is not new, with history as far back as Nikola TeslaâĂŹs research more than a century ago [23].Investigation into this topic has increased significantly recently and much progress has been made in establishing WPT as a technology in everyday use. Several techniques for accomplishing this have been established as dominant.

A review of the current state of the technology is desired, so the primary focus will be upon technologies that have already been introduced as commercial products, or are well along in the process of commercialization. There are many groups who

---

[1]Some companies are still in their early stages and thus have not released full details about their technology yet. The information in this table reflects all known publicly disclosed information at the time of writing.

Company	Method of Power Transfer	Max Power Delivered (W)	Approx. Range (ft.)
Cota	Concentrated Microwaves	1	30
Powermat	Inductive Coupling	5 to 50	Touching
uBeam	Ultrasound	Unknown (minimum 1.5)	3 to 13
WattUp	RF	10	15
Wi-Charge	Laser	10	30
WiTricity	Inductive Coupling	Scalable, on the order of 1000	7

Table 2.1: Comparison chart of wireless technology companies and their products' capabilities[1]

are researching this problem, but only a few are considered here. It is the aim of this chapter to introduce the few dominant technologies and to provide examples of their use in a public setting. To investigate all current research efforts that are underway would be neither feasible nor worthwhile; a brief examination of major contending technologies is sufficient to get an idea of the current thinking on the problem of WPT.

Mention companies that we are looking at Several groups have already made enough progress to commercialize WPT technologies. These entities have taken scientific research and taken advantage of certain aspects of those technologies to apply them to specific applications. This chapter will consider six such companies and discuss each one in detail. Powermat, Witricity, Wattup, uBeam, Cota, and Wicharge are the technologies under review, which will be compared according to several different metrics.

Specify gaps in the current technology Although the current body of knowledge has produced several techniques that are being pursued, there are limitations to those techniques that manifest as drawbacks.

Introduce time reversal Connect time reversal to gaps in technology

2.1 Characteristics of Importance

2.1.1 Why characteristics need to be defined

Different WPT technologies vary wildly in both their methods of operation and their
intended application. Further, certain measures of characterizing performance are
poorly defined in the field. For this reason, we will specify the working definitions
of several performance parameters important to comparing different wireless power
methods.

2.1.2 Range

This is simply the distance at which a WPT method can successfully transfer any
measurable level of power. It is important to note that this does not mandate any
level of efficiency. Thus, the maximum range at which a given technology is capable
of transferring some level of power will be larger than its actual operating range at
which it can transfer a sufficient amount of power. For this thesis, we will specifically
be referring to operating range. However, this does not do much to narrow down the
definition, and makes directly comparing two technologies very difficult, because each
company requires a different level of power at their receiver. Wavelength isnâĂŹt
used to characterize the range of different techniques, because different techniques
work under a wide range frequencies. In this thesis, techniques will be grouped under
three ranges, which are defined in Table 2.2.

2.1.3 Efficiency

Efficiency in particular is difficult to quantify, as there does not currently exist a stan-
dardized definition used by all parties. Each company defines it slightly differently,
and some have cited numbers without defining it at all. Efficiency of transfer can
include the amount of power drawn by the transmitter compared by the amount of

Class	Range
Short	Within 1cm of transmitting antenna
Medium	[RANGE HERE]
Long	[RANGE HERE]

Table 2.2: This table defines three classes of transfer ranges for the purpose of consistency. There does not currently exist any standard definition of ranges.

energy delivered to the target. It can also be defined as the transfer between antennas within a setup, with other losses (such as those due to rectifiers after transmission) being ignored. Where possible, we will specify which definition is being used.

2.1.4   Maximum Power

The maximum amount of power that can be transmitted to a target. This factor will limit the types of devices that can be powered by the technique. While high power transmission is not important for all devices, a larger range of power improves the flexibility of the technology.

2.1.5   Number of Devices

The scalability of the technique as a function of number of powered targets. Additional targets can impact other characteristics of transmission, such as maximum power or efficiency. Some technologies may perform better or worse as more targets are considered.

2.1.6   Active or Passive Transmission

TODO:...

2.1.7 Size and Weight of Transmitting and Receiving Units

TODO:...

2.1.8 Health Concerns

TODO:...

2.2 Technologies

2.2.1 Magnetic Induction

Of these, magnetic induction is perhaps most common, as it is used for electric tooth-brushes, shavers and charging mats. When current is passed through a metallic coil, a magnetic field is created in the environment around it in accordance with FaradayâĂŹs Law [19]. If another coil is positioned within this field such that the magnetic flow passes through it, the field induces a current in the second coil. The induced current can then be used directly or stored by the rest of the circuit [19]. This type of power transfer is simple to implement, but is constrained by its limited range and its need for precise coil alignment. The magnetic field must be as strong as possible to maximize the induced current. Unfortunately, the strength of such fields decreases is inversely proportional to their distance from the source. Furthermore, if the second coil is even slightly misaligned with the parallel of the magnetic flow lines, little to no current is induced in the wire [10]. [FIGURE]

In practical application, the range is limited to only a few centimeters with the maximum angle of misalignment being a few degrees [4]. These properties make magnetic induction an economical choice when a device can be simply positioned in direct contact with a charging device, as with electric toothbrushes and certain cell phones. Magnetic induction, then, while useful and simple, is best suited towards applications where extreme range limitations are acceptable. The technique cannot be generalized to work at longer ranges due to sharp decreases in efficiency, a drawback that WPT attempts to ameliorate.

2.2.2 Microwave Beaming

Fortunately, there are viable solutions to circumvent the practical pitfalls of magnetic induction. For example, microwave beaming is a WPT technique with perhaps the longest range of existing technology. Microwave beaming involves sending collimated microwave-frequency (1 GHz - 300 GHz) signals from transmitter to receiver [9]. These maser beams, when collected, are converted back into usable electricity by rectifying antennas [26]. Theoretically, beaming masers is extremely efficient because microwaves will self-propagate indefinitely in a vacuum, with no loss of energy. The presence of air means that some energy is always lost to dispersion<cite|check?>, though the practical range of the technique is still on the order of kilometers as opposed to centimeters. Unfortunately, serious challenges are still present to using microwave beaming as a feasible means of WPT. The first is that it requires high precision: if the beam does not strike the receiver, all of its energy is lost to the environment. Given the extreme ranges when microwave beaming would be considered, a small misalignment in transmission angle would result in the beam missing its target completely. Another concern is that the maser will be completely disrupted if anything, including the environment itself, blocks the path of the beam between the transmitter and receiver. This concern is compounded with the possibility that organisms and tissue could suffer damage from missed or blocked microwaves. Thus, microwave beaming only has applications in well-controlled or isolated environments such as laboratories, which can achieve extreme precision with minimal interference.

2.2.3 WiTricity

Whereas microwave beaming operates on the scale of kilometers and magnetic induction operates at the range of centimeters, highly resonant magnetic coupling (HRMC) by the Boston-based company WiTricity®is applicable on the scale of meters. This new method of WPT appears promising: WiTricity®self-reported 50% efficiency at two meters, followed by 10% efficiency at four meters [13, 24]. Demonstrations of HRMC have charged multiple devices without seemingly sacrificing overall efficiency

[13]: A 2009 study? showing powered relatively small devices - a phone and a televisionâĂŞ at a distance of about three or four feet [8], while a later 2012 study? showing powered electric vehicles. The public demonstrations by WiTricity®that HRMC can transmit power ranging from milliwatts to kilowatts, significantly more than was practical with traditional induction [13]. Though much is not explicitly known about the exact methods used by WiTricity®, there are a few indications about the underlying system. First, it is known that HRMC tunes both the transmitter and receiver circuits to the same resonant frequency, a concept analogous to tuning two instruments to the same pitch, to generate a greater voltage at the receiver when compared with traditional induction. The power entering the transmitter generates a broadly distributed magnetic field, which radiates outwardly enough to encompass multiple receivers. Second, this property of HRMC can additionally be used to increase working range through relays, devices with a strong mutual inductance, which can recreate the magnetic field with minimal loss. [4]. Finally, an additional technique used to actively adjust the resonance and impedance of the networks so that transmission remains optimal [13]. This technique, impedance matching, minimizes the amount of wave reflection inside the transmitter and receiver circuits, ensuring that most of the energy is actually passed to the load component. This process requires a constant proprietary feedback mechanism to optimize the receiver for the given distance from the transmitter. Though their methods are complex and burdensome, WiTricity®has achieved impressive results. While HRMC looks very promising in the coming years for commercial applications, the method is not without its drawbacks: it is likely to be prohibitively expensive for residential use and the range is still reasonably limited to only a few meters. Thus, there is still no safe wireless charging method which can efficiently transmit energy over a distance greater than four meters.

2.3 Time Reversal

Team TESLAâĂŹs project hopes to overcome some of these limitations through a novel method: the use of electromagnetic time reversal (TR). TR is a proven tech-

nique in signal processing, with applications in acoustics as well as electromagnetics. Though its publicity is limited, there is a wealth of available literature regarding TR in certain specialized areas. Here we briefly describe the development and historical applications of the technique to illustrate where TESLAâĂŹs project will expand this literature. Time reversal as a technique was first developed in the 1990s. Some of the earliest and most influential work was conducted through teams led by Mathias Fink and Claire Prada of the University of Paris. These researchers used the technique to focus sound waves on âĂIJscatterersâĂİ, objects that reflect the pulses [15]. An array of transducers would fire a sonic pulse into some propagation medium and listen for the echo. The recording of that echo was reversed in the time domain and transmitted back into the medium. They repeated (iterated) this process, causing the acoustic signature of the strongest scatterer to appear more prominently each time. In this way, the team was able to iteratively focus on the scatterers without needing prior knowledge of their location. Prada and her team submitted this DORT (French acronym, English: Decomposition of the Time Reversal Operator) method as a process for finding cracks or faults in structural members [15]. More importantly, Prada et al. went on to demonstrate that the method could always resolve the brightest scatterer if given enough iterations, that it worked better in a heterogeneous medium than a homogenous one, and that it was both experimentally and mathematically possible to resolve multiple targets at once [16]. These discoveries generated significant interest in a subset of the acoustics research community. Others in the field of acoustics went on to refine the DORT method as an imaging technique, and as the field gathered attention, further explored formalizing the problem in general. An excellent example of the latter is the theoretical work by D. H. Chamber in his 2007 examination of TR for target detection and characterization [5]. In 2010, Nguyen and Gan developed a way to extract much more information from an anisotropic (directionally distinct) scatterer, including its rough shape, density, and radius. In doing so, they developed a faster mathematical approach to locating their scatterers that relied on several good approximations instead of one exhaustive computation [14]. Also in 2010, Barbieri and Meo made a large contribution to the field by bringing

together the DORT method, which works in linear environments, and another similar method for working in nonlinear environments. This allowed them to resolve and distinguish between linear scatterers such as holes and nonlinear scatterers such as cracks [3]. Imaging is not the only application for a focusing method, however, and others adapted the existing body of TR research to new problems. The reciprocity of the wave function that Fink and Prada relied on to develop the technique holds for all waves it can be used to model âĂŞ this means that the time reversal operation works much the same way with electromagnetic waves as it does with sound waves [5]. This was explored as early as 1999, but was largely concerned with the same imaging problems occupying those in acoustics until at least 2007 [5]. However, that gradually began to change. In 2011, a team including graduate students from the University of Maryland posited that time reversal was an ideal mechanism for wireless communication [8]. In the same way that a sound wave could be made to collapse on a scatterer, they showed that an information packet could be made to collapse on a receiver. The team submitted this as a âĂIJgreenâĂİ or eco-friendly communication method, because information could be tightly concentrated at a single point rather than beamed wastefully in all directions [8]. Later, this same property was examined for its security benefits instead of its environmental ones. In February of 2013, a team of researchers at the University of Maryland, including Matthew Frazier and Steven Anlage, published a study discussing TR as a method to selectively send information in a chaotic wave environment [6] [21]. Essentially, the team was able to create an exclusive communication link to a certain object, without needing to know its location, and without interfering with nearby objects. In their experiment, they were able to transmit data (in the form of images) exclusively to a desired port, while the other port received only nonsense. Beyond its practical applications, in the process, Frazier and his team used nonlinear elements to extend TR in new and exciting ways. Recall that in traditional TR many iterations are required to pinpoint the target. The addition of a significantly nonlinear element greatly simplifies the pinpointing process. When a wave strikes the element, harmonic frequencies are produced at integer multiples of the original frequency. These harmonics can be quickly located

25

in the echo's frequency domain and filtered to select them exclusively. The important distinction is that since the harmonics originated directly from the target, all subsequent broadcasts of the TR signal will collapse there exactly without the need for iteration [6]. Frazier and the others put forth several exciting directions to pursue with this concept: the aforementioned secure communication channels, hyperthermic treatment of tumors, and a long range WPT system that eschews traditional high power beams. It is this last area that TESLA intends to explore.

TODO:WPT history and state of art TODO:TR history and state of art

Chapter 3

Methodology for Conducting Linear Time Reversal

TODO:...

Chapter 4

Overlapping Sonas

TODO:...

Chapter 5

Spatial Profiling

TODO:...

Chapter 6

Moving Reconstructions

TODO:...

Chapter 7

Numerical Simulations of the Nonlinear Time Reversal Process

7.1 Purpose

In this chapter, we focus entirely on numerical simulations of NLTR as they apply to WPT. Our focus was threefold: (1) simultaneous NLTR collapse onto two nonlinear objects simultaneously (2) selective collapse of NLTR onto two distinct nonlinear objects and (3) characterize the transmission efficiency of the process. From these three focuses, we showed the NLTR process may be generalized to an arbitrary number of nonlinear objects in an enclosure and that these reconstructions may be selectively rectified at the nonlinear objects. We provide a scheme to characterize the efficiency of our process but were unable to develop a theory for tuning the efficiency. Our results provide a fundamental baseline for developing an experimental algorithm for targeting objects in an enclosure for WPT applications, either selective or non-selectively. We will first discuss the general scheme used for performing NLTR followed by the setup, experimental results, and discussion for each of our three focus topics.

The process of developing a new technology required benchmarking each step diligently. Any successful WPT technology must have very high effective transmission efficiency, implying minimal loss in each step of the system. Given the broad frequency signals used in experimentation, a significant drawback to any TR experiment is

the inherent wave reflection at interfaces between equipment, various mediums, or circuitry [19, 10]. While wave reflection losses can be theoretically be measured via S Parameters (explained later) of an experiment, these sources of loss are not practically measurable due to the fact that measuring the losses would create addition interfaces in the system, introducing additional sources of wave reflection [19]. To calculate the true ceiling on effective transfer efficiency, it is necessary to numerically simulate the process, as a simulation can calculate the various losses without interfering with the system itself.

In addition to using simulations to study the sources of loss in our system, it also provided us with a simple nonlinear element–a model diode. As explained in previous chapters, the nonlinear response of in our Gigabox experiments was found to be difficult to excite due to power limitations, noise, or equipment sensitivity. The difficulties that we encountered in our physical experimentation were circumvented by numerical simulating the NLTR process. By being able to monitor the voltage and current response of the diode at all times in the simulation, we were able to troubleshoot problems that occurred in the numerical NLTR process that would have otherwise have been impossible to determine in experimentation.

7.2   Methodology

7.2.1   Equipment

In order to perform these tests that were not possible in the Gigabox, we used the program Computer Simulation Technology: Microwave Studio (CST for short) to perform electromagnetic wave simulations. CST is an industry standard modeling program that uses the Finite Integration Technique (FIT) to numerically solve Maxwell's equations [22]. This technique is a generalized version of the well-known Finite Difference Time Domain (FDTD) method but can resolve complex geometries and boundary conditions in a simpler manner. We will not discuss these techniques at length, as they are well-understood in the literature [17], [25]. Our team had two comput-

ers with a total of two shared CST licenses to perform simulations. The processing power, RAM, and GPU availability are shown below in Table 7.1. CPU A was used for either single simulations or computationally small simulations. A single simulation refers to a simulation where we did not sweep a parameter. CPU B was used for large simulations or parameter sweep simulations, requiring either large amounts of memory or large amounts of time, respectively. In general, we used CPU A to perform NLTR and selective NLTR while we used CPU B to calculate transfer efficiency and characterize nonlinear response characteristics.

	CPU A	CPU B
Processor	Intel Xeon CPU X5670 @ 2.93 GHz	Intel Xeon CPU E5-2680 @ 2.50 GHz
Number of Processors	2	2
RAM	44 GB	128 GB
GPU Available	No	Yes

Table 7.1: Technical specifications of the computers used for conducting all simulations and modeling.

7.2.2 Time-Reversal and Nonlinear Sona Extraction

To start any simulation, we first generated a Gaussian pulse signal in MatLab. For this interrogation signal, we chose the amplitude, center frequency, and bandwidth frequency for our experiment. An example input signal is shown inset in Figure 7-1. The simulation was run using this pulse signal, noting one of the ports as an injection port (e.g. Port A) and one as the recording port (e.g. Port B).

In general, we had two methods to extract the nonlinear sona from our recorded signal: (1) applying a Fourier transform and band-pass filtering the raw signal and (2) pulse inversion. As previously discussed, many of the Gigabox experiments were performed by recording a sona, applying a Fast Fourier Transform (FFT), and finally using a band-pass filter on the recorded signals to extract the harmonic signal at
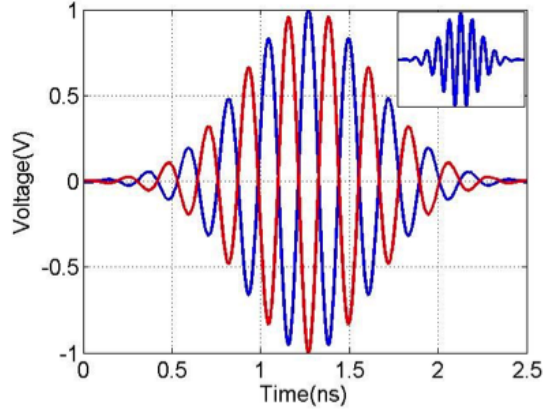
Figure 7-1: This shows our input waveform with a 4.4GHz center frequency and 1.0GHz bandwidth. The blue signal is the non-inverted input and the red signal is the inverted input. A singular, non-inverted waveform is shown in the inset.

the correct frequency. In our numerical simulations; however, the sonas were only recorded for 30–35 ns and the discretized nature of the data on this time scale led to distortion of the sona signals. The team also explored using another method of sona extraction that has been well documented in the literature [18], [12]. Hong et al. have used this method for numerous time-reversal experiments, citing its computational simplicity as a benefit for using it in physical experiments [12]. The process involves summing two signals, rather than applying a transformation to an entire sona signal, saving time. While this process proved to be very difficult for our Gigabox experiments, it was quite efficient at producing the nonlinear sona in CST. Due to the simplicity of pulse inversion, we used this method for extracting all nonlinear sonas. In this method, we ran the same simulation once with our original input signal and then we ran it a second time with an inverted version of our original signal. Inversion simply means that the entire original signal was multiplied by −1. Assuming a linear system, the sum of the original and inverted signals sums to 0; however, a nonlinear system sum is non-zero. Because the diode is the only nonlinear portion of the system, summing the original and inverted signals yields only the signal from the diode, which is the desired nonlinear sona. TODO:Need to annotate figure with a,b,c,d Figure 7-2(a) and (b) illustrate two sona signals, where the blue signal is the non-inverted sona and the red signal is the inverted sona. Figure 7-2(b) contains a
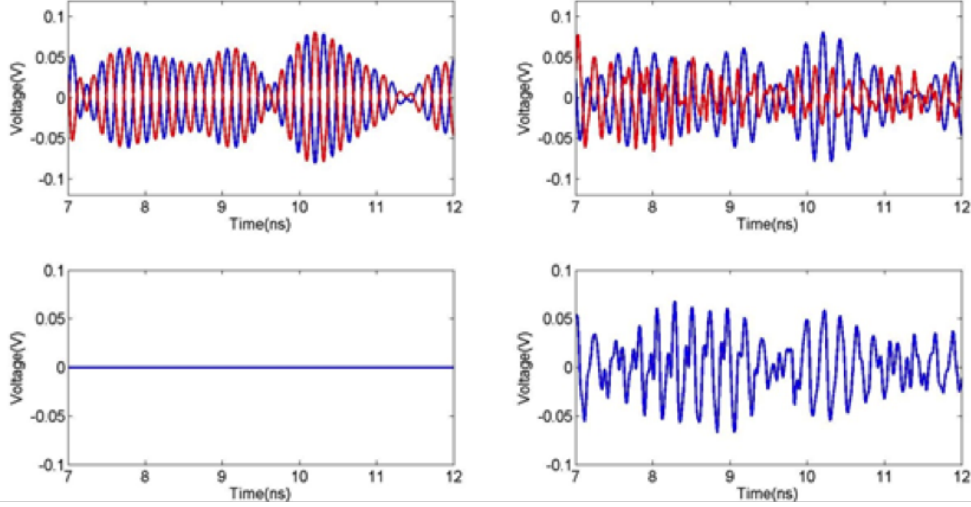
38

Figure 7-2: (a) shows a portion of the non-inverted (blue) and inverted (red) recorded response signal. (b) shows the same two response signals when a diode is present in the simulation. (c) the sum of the two signals in (a), resulting in signal annihilation. (d) the sum of the two signals in (b), which produce a non-zero signal.

nonlinear element while 7-2(a) does not. The corresponding (c) and (d) show the result of summing the two signals. It is clear that total annihilation of the sona signal occurs when no nonlinear element is present, as in 7-2(c), while a clear signal is present in 7-2(d).

This method to extract the nonlinear sona was chosen over taking the FFT and filtering the recorded signal as sample rate for the simulation data was not high enough to ensure the results would not be distorted. This discretization of data caused the resulting time-reversed sonas to produce incorrect results using the FFT and filter method, while the time-reversed sonas produced correct results with the pulse inversion method.

7.2.3   Defining and Controlling the Nonlinear Element

In the simulations themselves, we used a model diode as our nonlinear object, as it has a nonlinear I-V curve. The diode location for each simulation was chosen semi-arbitrarily with the only restriction to not be within 1–2 wavelengths of either port, as this may have created near-field effects that influenced the results. In CST, the diode component is modeled as the following circuit (Figure 7-3) and mathematical
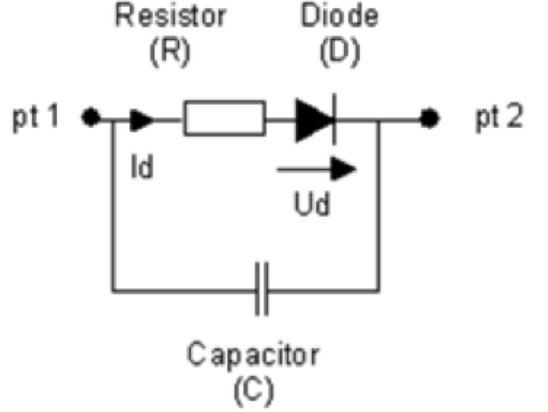
Figure 7-3: CST circuit model of a diode.

relationship (Equation 7.1 and 7.2). From these, the user may change the parasitic capacitance (C), the series resistance (R), the reverse conductance (G_s), and the functional temperature (T).

For $V_d > 0$:

$$I_d = I_0 \left(e^{\frac{eV_d}{kT}} - 1 \right) = I_0 \left(e^{\frac{V_d}{V_k}a} - 1 \right) \tag{7.1}$$

For $V_d < 0$:

$$I_d = G_s V_d \tag{7.2}$$

To obtain idealized results, we set C and G_s to 0, as these values reduced the magnitude of the nonlinear response. We used the default $R = 50\Omega$, as very large R reduced the overall signal greatly and a very small R did not produce any harmonics. This left only T to tune the I-V curve of the diode. In real life, different diodes have different I-V curves based on material. In order to simulate these differences mathematically, we changed the temperature of the diode in the simulation, as shown in Figure 7-4.

In reality, this changed the knee voltage (V_k) for the diode. We chose V_k to be the applied voltage needed to achieve a current of $0.2I_0$. The parameter a is used to define this $0.2I_0$ cutoff. As discussed later in this chapter, we will show how the nonlinear response of a diode is dependent on both the input pulse amplitude and the
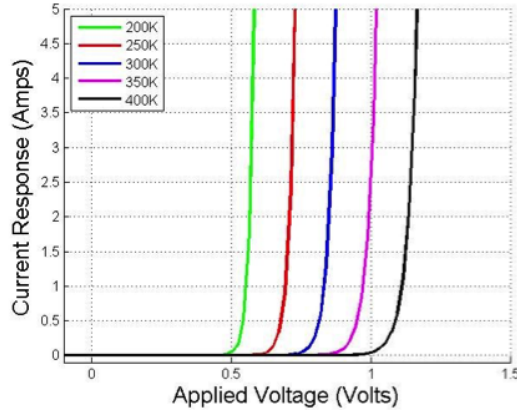
40

Figure 7-4: Different I-V curves that can be modeled in CST. It should be noted that the "Temperature" of the diode only changes its mathematical definition of the I-V curve

knee voltage. This nonlinear response was maximized to allow for selective targeting between two diodes simultaneously.

7.3 Results

7.3.1 Simultaneous Nonlinear Time Reversal

The first focus of our numerical simulations was to illustrate the collapse of time-reversed nonlinear sonas on multiple targets simultaneously. To be an effective WPT system, our technology would need to be able to charge more than one device at a time. Based on literature illustrating NLTR collapsing on a single nonlinear object, we hypothesized that a nonlinear sona would collapse on an arbitrary number of nonlinear objects if the nonlinear objects were present in the time-forward step of NLTR [7, 6]. We assumed that the reconstruction on each nonlinear object would sum linearly and independently such that no reconstruction would interfere with another, as shown in Equation 7.3, where R_i is the reconstruction on a single nonlinear object and x_i is a weighting of the amount of power that the single nonlinear object contributes to the overall power of all reconstructions. Based on this, we expected the reconstruction waveforms of the independent single-diode simulations to match a single, multi-diode

simulation.

$$R_{tot} = \sum_i R_i x_i \tag{7.3}$$

This feature was realized by creating a geometry with two diodes present along with two ports to record and emit signals, shown below. We created a quasi-two-dimensional (2D) irregular cavity in CST. This cavity was a 15cm x 15cm x 0.76cm square box modified with various circular and elliptical segments removed from the walls as shown in Figure 7-5. The 0.76cm height was chosen to maintain a 2D simulation. Equation refeq:numerical-cutoff-freq was used to calculate the cutoff frequency for the fundamental mode of a parallel plate cavity, below which only 1 frequency will propagate, reducing the time needed to simulate [10].

$$f_c = \frac{c}{2h} \tag{7.4}$$

Using a cavity of height 0.76 cm resulted in a cutoff frequency of 20 GHz, well above our typical test frequencies of 4-5 GHz fundamental and 8-10 GHz harmonic. We chose this cutoff frequency in the event we needed to use a higher fundamental frequency to create better spatial resolution of our reconstruction. The area dimensions for the Cut Box Model were chosen to minimize computational time while still maintaining a reasonable mode density, as shown in Figure 7-5(a)TODO:need to annotate figure. This mode density is required to allow the ray chaotic environment to have high sensitivity to initial and boundary conditions; a low mode density will prevent NLTR from having high spatial resolution.

We used two Teflon-coated dipole antennas to emit and record signals [11]. Two diodes are placed inside the cavity, shown by the blue circles in Fig. 5. A 4.4 GHz center frequency pulse with a 1.0 GHz bandwidth was chosen to minimize the reflected power and applied to antenna A. The interrogating pulse is shown as an inset in Figure 7-5(a).

The specific frequency and bandwidth was chosen for this geometry to minimize initial wave reflection (S_{11}) into the enclosure. Figure 7-6 shows that using a 1
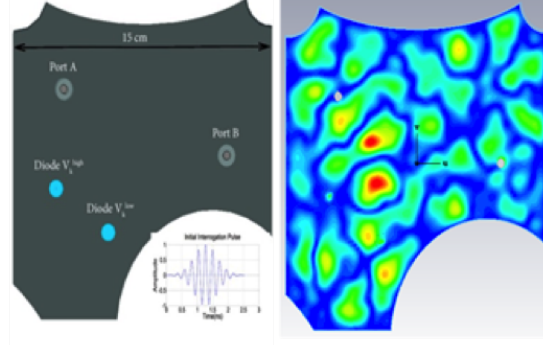
Figure 5: The cut-box simulation geometry used in CST. (a) shows the location of the 2 ports (A and B), 2 diodes (V_k^{high}, V_k^{low}), length scale, and the lower inset shows the initial interrogation pulse. (b) shows the electric field at a point in the simulation, illustrating the limited excited mode density.

Figure 7-5: The Cut Box simulation geometry used in CST. (a) shows the location of the 2 ports (A and B), 2 diodes (V_k^{high}, V_k^{low}), length scale, and the lower inset shows the initial interrogation pulse. (b) shows the electric field at a point in the simulation, illustrating the limited excited mode density.
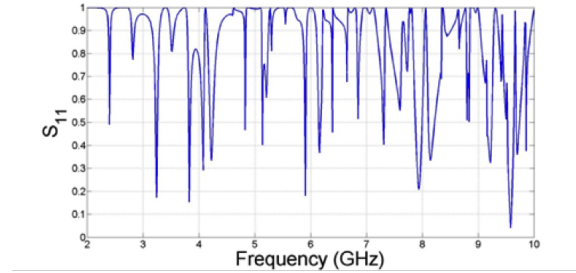

Figure 7-6: The S_{11} spectrum for the Cut Box Model. We wanted to minimize S_{11} for our simulation while maintaining a large bandwidth. This led to choosing a 4GHz center frequency with a 1GHz bandwidth.

GHz bandwidth, an optimal center frequency is 4.4 GHz. The dips in the S_{11} value represent optimal frequencies to use, as a low S_{11} indicates a large portion of the signal entered the cavity. The large number of peaks is indicative of the mode density of the geometry, where low frequencies are sparse given the relatively small scale of the cavity.

Using this input pulse and the pulse inversion method of sona extraction, we were able to perform NLTR in the Cut Box Model. By measuring the observed voltage and corresponding current during the time-reversed step, we measured the quasi-power over time in each diode. As shown in Figure 7-7, the reconstruction waveform on
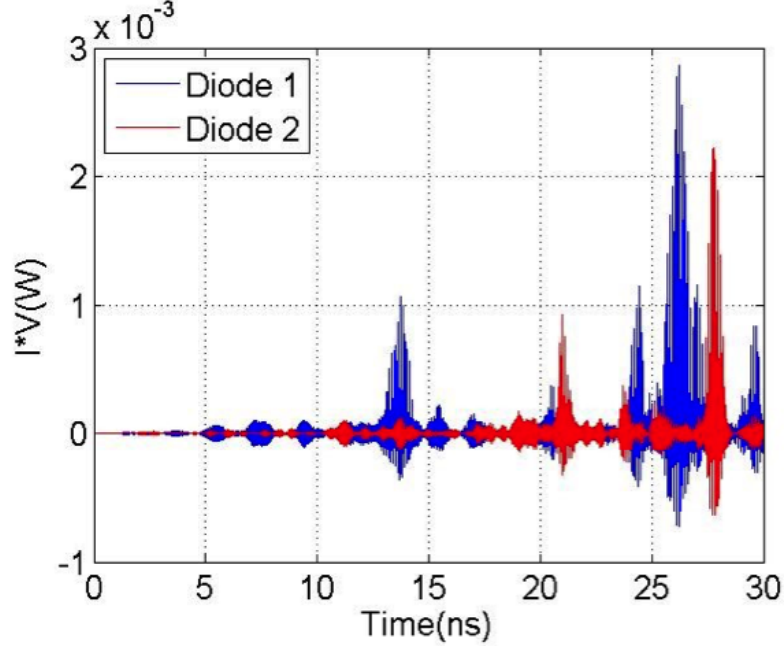
43

Figure 7-7: The time-reversed reconstruction on two diodes simultaneously performed inside the Cut Box geometry.

each diode matches the expected results for a 1-diode experiment [21, 3].

7.3.2 Discussion of Simultaneous Nonlinear Reconstructions

This result alone signifies the generality of NLTR whereby any nonlinear object in the cavity will observe a reconstruction in the time-reversed step. In regards to a larger WPT system, one can imagine that this is particularly useful inside of a home or public area, where any device may be powered as long as it is within range of the transmitter/receiver base station. Because the process used only creates a reconstruction at the nonlinear element, it is as simple as repeating the NLTR process rapidly, creating a quasi-pulse width modulation (PWM) signal that can charge a battery. PWM is a method for controlling how active a device is by rapidly switching the device on and off. For example, a fan has different speeds because it operates 25%, 50%, 75%, or 100% of the time. Similarly, if we can reconstruct on a battery circuit every 10% or 20% of the time, we can effectively charge the battery. As soon as the nonlinear object leaves the enclosure, it will no longer receive power. By having a base station that can actively modulate output sona power, it would be very simple to

44

change the amount of power transferred to each device. This dynamic power control is outside the scope of our project but represents a much later extension to this WPT system.

7.3.3 Simulation of Selective Collapse of NLTR

The logical next step is to determine how such a system would be able to determine which device should be powered. As previously shown, if nothing is done to alter the sona signals, then the sona from each nonlinear object will sum linearly and produce reconstruction at all nonlinear objects in the time-reversed step. Given that each reconstructions sums independent of one another, we hypothesize that we should be able to eliminate the contribution of one nonlinear reconstruction to the overall set of reconstructions without altering the fidelity of the any other individual reconstruction on other nonlinear elements. For example, in an enclosure with 3 diodes, if we could suppress the response of diode 2 in the time-forward step, then we would expect to only observe a reconstruction on diodes 1 and 3, creating a selective targeting method. Using Eq. 3, this would imply a weight of $x_i = 0$, as shown in Equation 7.5.

$$R_{tot} = \sum_i R_i x_i = R_1 x_1 + R_2 x_2 + R_3 x_3 \qquad (7.5)$$

TODO:How does this imply xi=0?TODO:why does this stop at 3 specifically? Should it go on to x_i? If so we need $2 + ... + i$.

In a commercial setting, this would be an extremely useful aspect to our WPT system, as companies could require payment to use the system and would otherwise suppress the reconstruction on the user's device. The fact that the nonlinear object is passive in the environment implies that this selective targeting could even be used to "resurrect" a dead phone, a feature not seen on any current WPT technology on the market.

We have developed a method of performing such a targeting scheme based on the previously mentioned diode model. In the simplest case, we show that selective targeting for 2 diodes with two separate voltage knees was obtained (noted V_k^{high} and
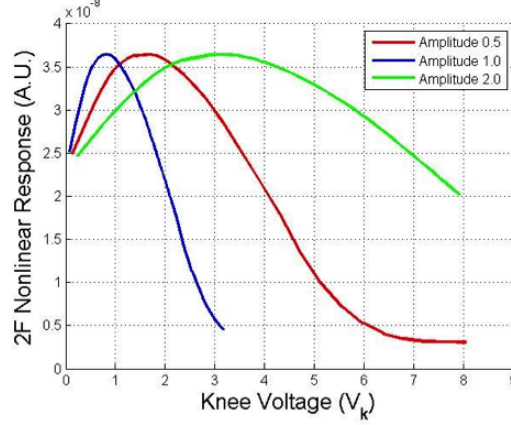
45

Figure 7-8: The nonlinear response of the diode had a clear maximum at a specific knee voltage. By using a pulse amplitude that corresponded with the specific diode knee voltage, we could selectively target diodes in CST.

V_k^{low}).

Recall the current response in the diode from Equation 7.1. One useful aspect to the diode definition function is that if $V < V_k$, then the diode has very little current response, which in turn implies a low nonlinear response. We utilize this characteristic while performing selective targeting on a low V_k diode. Similarly, we observe that at small V_k values, the nonlinear response is small. These two observations led to the hypothesis that nonlinear response may be maximized given an initial pulse by selecting a proper V_k value. As shown below, Figure 7-8 was obtained by sweeping over many V_k values for different initial pulse amplitudes given the same geometry and process conditions as previously stated. Given this distribution, we may target a high V_k diode, as the nonlinear response will be stronger in the high V_k diode than the low V_k diode.

To perform this selective targeting, we once again used the Cut Box Model. In the simplest case, we consider selective targeting of a low $V_k = 0.79V$ (V_K^{low}) diode at the exclusion of a high $V_k = 6.60V$ (V_k^{high}) diode. Given the large value of V_k^{high}, we expect to see no response in that diode while maintaining a reasonable nonlinear response in the V_k^{low} diode. We used a pulse with amplitude $V = 1.0V$ during the time forward step, emitted at Port A in Figure 7-5(a). Using pulse-inversion, we extracted the nonlinear sona from the recorded signal at Port B, time-reversed the signal, and
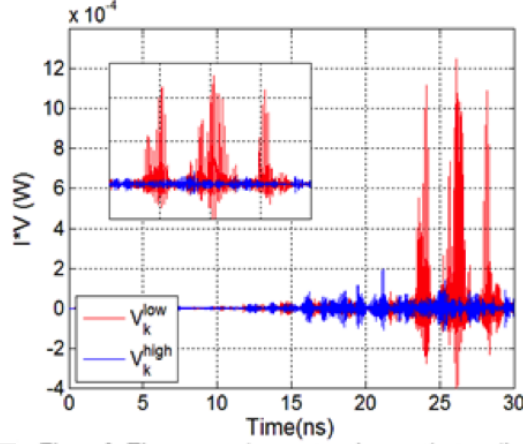
46

Figure 9: Time-reversed reconstructions on the two diodes while targeting V_k^{low}. Very little signal is seen on the V_k^{high} diode. The insert shows the details of the reconstructions between 22 and 30 ns.

Figure 7-9: Time-reversed reconstructions on the two diodes while targeting V_k^{low}. Very little signal is seen on the V_k^{high} diode. The insert shows the details of the reconstructions between 22 and 30 ns.

re-emitted it from Port B. Figure 7-9 shows the time-reversed reconstructions on both diodes. This results in a reconstruction almost exclusively on the V_k^{low} diode during the time-reversed step. The presence of three reconstructions when only one initial pulse was TODO:missing is not alarming, as short-orbit paths between Port A, the diodes, and Port B that carry enough power to excite the diode harmonics are known to exist [20]. To calculate the quality of the selective reconstruction, we determined the aspect ratio by comparing the max of IV on both diodes. For this scenario, we calculate a power delivery aspect ratio of 6.35:1 for the V_k^{low} diode relative to the diode with V_k^{high}.

The more difficult scenario was to selectively target a high V_k diode at the exclusion of a low V_k diode. We utilized the peak in nonlinear response as a function of knee voltage from Figure 7-8. By choosing the correct pulse amplitude corresponding to a peak value that was matched to the high V_k value, we expected to see the strongest nonlinear response from that specific diode, resulting in a stronger reconstruction. In this scenario, the low V_k diode will still observe a reconstruction; however, it will be smaller in amplitude than the high V_k diode reconstruction. Given that a real system would involve a rectification circuit in addition to the diode, the smaller amplitude

47

Figure 10: Time-reversed reconstructions on the two diodes while targeting V₁ʰⁱᵍʰ. Sona amplitude modulation resulted in a clear contrast between the two signals.
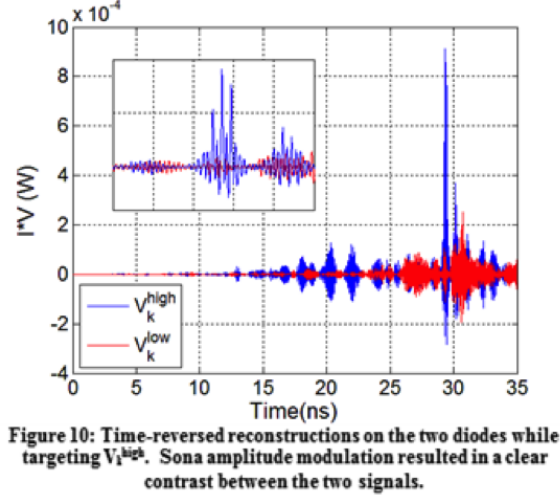
Figure 7-10: Time-reversed reconstructions on the two diodes while targeting V_k^{high}. Sona amplitude modulation resulted in a clear contrast between the two signals.

reconstruction may not be able to turn on the rectifier while the high amplitude reconstruction at the high V_k diode would turn on. For our simulations, we were able to model this by measuring the observed power (IV) on the diode and modify the sona amplitude in order to ensure the V_k^{high} diode had rectification while the V_k^{low} diode did not.

For this second scenario, with $V_k^{high} = 2.22V$, we once again used an amplitude $1.0V$ pulse during the time-forward step so that we may compare the results from both scenarios equally. As shown in Figure 7-10, pulse amplitude of 1.0 has a maximum nonlinear response at $2.22V$. We chose this V_k value, as it gave the clearest reconstruction. Once again, we used pulse-inversion to extract the nonlinear sona. In general, this results in a larger magnitude reconstruction on V_k^{high}. This contrast between the V_k^{low} and V_k^{high} reconstructions was amplified by modulating the time-reversed sona amplitude, such that the reconstruction voltage seen at the target diode was barely larger than V_k for V_k^{high} and just barely smaller than V_k for V_k^{low}. This resulted in selectively reconstructing on V_k^{high} only during the time-reversed step with an aspect ratio of 3.61:1 for the V_k^{high} diode relative to V_k^{low}, as shown in Figure ??TODO:Which ref?.

48

7.3.4 Discussion of Selective Nonlinear Time Reversal

We have demonstrated a basic method for creating selective rectification using NLTR to target different nonlinear objects. This represents a stepping stone from the previously shown method of generalizing NLTR. By altering the input pulse amplitude, we were able to achieve the hypothesized nonlinear response suppression of specific nonlinear elements. This shows that the nonlinear reconstruction created on each nonlinear element is independent of one another and may be modified without impacting the other elements of the overall reconstructions. We have shown that this WPT technology would be capable of ubiquitous charging or any nonlinear device as well as selective targeting of specific devices. One may think of this as having an NLTR charger in one's home compared to having an NLTR in a business. In a domestic setting, there is very little need to restrict access to power. There are many outlets in one's home and there is no need to tell someone they are not permitted to use it. In a business however, a power outlet is not available to customers unless they pay for it. In this case, it is very useful to be able to selectively choose who may receive power. Although we have not shown a full-fledged system to do so, we have presented a foundational process that may be improved upon in order to create a successful NLTR-based WPT system.

7.3.5 Simulation of Transmission Efficiency of NLTR Process

We have so far shown that NLTR may be used in a WPT system to either power all nonlinear objects or selectively target the nonlinear objects within a relevant range. One significant question though that arises is to what efficiency are these objects powered. Surely a system that can only transfer 2% of applied power will not be a successful WPT technology, as the consumer is paying for the luxury to not carry around a cable. If the user has to pay 50x more for the power they are very unlikely to use our system. As previously discussed, energy losses are often difficult to calculate in real experiments due to wave reflection and other systematic sources of error. However, by simulating the NLTR process, we are able to observe approximate
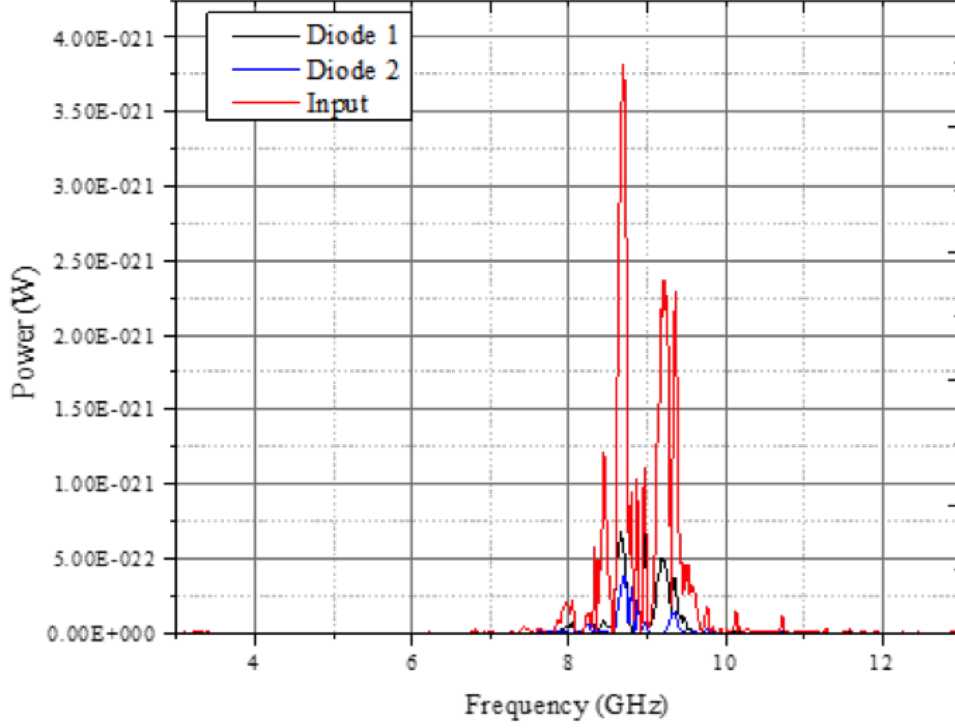
Figure 7-11: A typical power spectrum obtained in the time-reversed step (reconstruction). The power that enters the diodes only represents a portion of the overall power input in the simulation.

transfer efficiency. In CST, we are able to track power input and power loss via wave reflection, absorption in both lumped elements and environment materials, and radiation loss at another port. One drawback to using the built-in CST power tracking is that everything is recorded in the frequency domain rather than time domain. For example, a typical power spectrum from a time-reversed step of a 2-diode NLTR simulation is shown in Figure 7-11. As we are interested in overall power input compared to overall power output, we used this data along with Equation 7.6 to compute the efficiency of transfer in our simulations.

$$e = \frac{\sum_i P_{i(diode)}(f)}{\sum_i P_{i(input)}(f)} \cdot 100 \tag{7.6}$$

The above data was taken from a simulation run in the Cut Box Model for the previously discussed two-diode simultaneous reconstruction. For this simulation, we found that 18.6% and 7.3% of power were transferred from the nonlinear sona to

50

(a) Illustrates the geometry of the simulation.

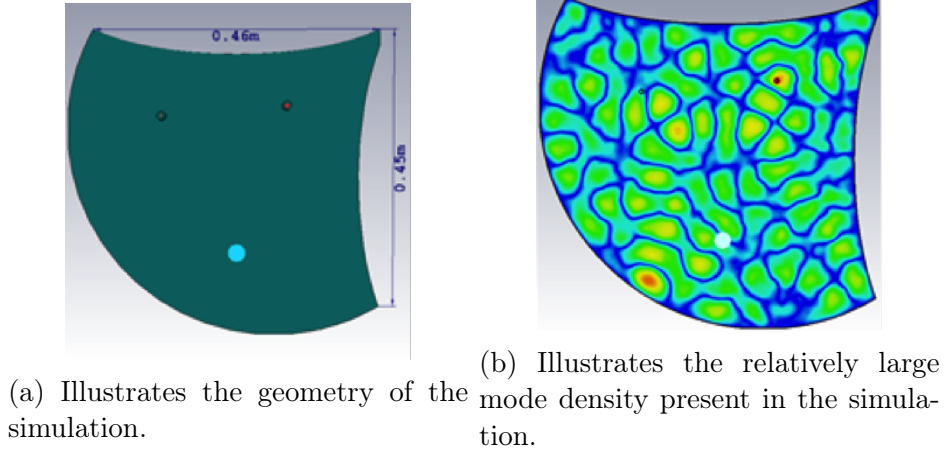(b) Illustrates the relatively large mode density present in the simulation.

Figure 7-12: The room model

diodes 1 and 2, respectively. This provides a promising outlook.

Our next question was whether or not these transfer efficiencies were a function of distance between transmitter port, diode, and receiver port. We found that using similar diode positions as previously stated resulted in transmission values around the 7–18% shown above. We decided to introduce a new model with a much larger length scale, called the Room Model shown in Figure 7-12.

We chose to use a 45cm x 45cm x 0.76 cm initial box to simulate a large geometry while still maintaining a quasi-2D cavity. The 45 cm length scale was used, as any larger simulation would run out of memory. Due to the length of simulation and decreased nonlinear signal strength, this model was unable to be used for further efficiency calculations. From Figure 7-12, the distances in the simulation are much larger than the Cut Box and may be used in the future to determine whether transmission efficiency of NLTR is dependent on distance between transmitter, nonlinear object, and receiver ports.

7.4   Conclusion

Using CST, we have successfully demonstrated our 3 goals: (1) simultaneous reconstructions on multiple nonlinear objects (2) selective reconstructions between multiple nonlinear objects and (3) calculation of a baseline transmission efficiency of NLTR.

For simultaneous and selective targeting, we provide a basic framework to perform these processes using numerical simulations; however, these processes are still yet to be performed in real-world experimentation. We believe that this illustrates a foundational work for future experiments to demonstrate the feasibility of these features in a new WPT technology. Additional research must be done in order to characterize the ceiling on transmission efficiency if NLTR is to be applied to a future WPT technology.

Chapter 8

Nanorods

TODO:...

Chapter 9

Rectification

9.1 Goals of Rectenna

One of the main components of any WPT system is its rectifier, as it performs the crucial step of capturing the broadcasted energy and transforming it into a usable form. To accomplish this, a rectenna, a dual-purpose device that combines an antenna and a rectifier, is necessary. The antenna picks up the unusable, oscillating AC signal received from the transmitter, the rectifier converts the signal to relatively stable DC power, and this usable power is passed to an arbitrary load.

In addition to standard rectification, the rectenna must serve as a passive nonlinear element. In NLTR, a nonlinear element is required to produce harmonics from the initial interrogation pulse broadcast by the transmitter. However, this goal is secondary to the main purpose of rectification.

The rectenna was designed to fit the following parameters. First, the rectenna must operate efficiently at the high frequency (1–10 GHz) required for efficient NLTR. Additionally, losses due to reflection and parasitic effects within the antenna should be minimized. Finally, to fulfill the role of a nonlinear element, the rectenna should generate distinguishable harmonics strong enough for the purposes of NLTR.

In short, to rectify and generate harmonics for NLTR, the rectenna must be capable of not only efficient rectification at high frequencies, but also production of strong harmonics for NLTR.

9.2 Diode Selection and Testing

The diode is the most important single component to consider for the rectenna, as it is the main rectifying component. Careful consideration of its characteristics is vital. The switching frequency, forward voltage drop, and impedance of the diode are of particular importance to the desired goal of efficient rectification.

For the rectenna in our design to perform efficiently, the diode must satisfy several requirements:

The diode must maintain functionality as a diode at a transmission frequency of 1–10 GHz, and must rectify at a frequency of at least 10 GHz. This requirement severely limits the possible choices for the rectenna diode. The frequency of a diode is inversely related to its reverse-recovery time (TRR), the fastest time the diode can switch from forward to reverse bias [?].In traditional P-N junction diodes, minimum TRR is on the order of tens to thousands of nanoseconds, even for fast diodes [?]. In a high frequency circuit, a P-N diode would be no different than a short circuit, and no rectification would occur.

The diode must have the lowest forward voltage drop possible. The voltage drop represents the reverse bias that remains when the diode works in the forward direction, and can be a significant contributor to power loss. The team's experimental WPT capabilities are limited to fairly low voltage microwave signals (.5 V to 1 V signal amplitude), which makes forward voltage drop especially important.

Finally, impedances should be minimized to reduce loss. All diodes have intrinsic impedances such as parasitic capacitance and resistance. Impedances contribute to losses during rectification and destabilize circuit behavior, resulting in unpredictable behavior.

Considering these factors, a Schottky barrier diode were chosen for the rectenna. Unlike P-N junction diodes, Schottky diodes have extremely low TRR and low forward voltage [?]. Schottky diodes do have a lower maximum reverse voltage rating, higher reverse leakage current, and higher cost than P-N diodes. However, these are relatively minor issues in our application. A Schottky `MA4E1317` diode was used as the rectifying

diode. The diode parameters from the are shown in Table 9.1.

Test Conditions	Symbol	Units	Min.	Typ.	Max.
Junction Capacitance at 0 V at 1 MHz	Cj	pF	-	.020	-
Total Capacitance at 0 V at 1 MHz	Ct	pF	.030	.045	.060
Junction Capacitance Difference	DCj	pF	-	-	-
Series Resistance at $+10\ mA^2$	Rs	Ω	-	4	7
Forward Voltage at $+1\ mA$	Vf_1	V	.60	.70	.80
Forward Voltage Difference at $+1\ mA$	DVf	V	-	-	-
Reverse Breakdown Voltage at $-10\mu A$	Vbr	V	4.5	7	-
SSB Noise Figure	NF	dB	-	6.5^4	-

Table 9.1: Datasheet for the M/A-Com `MA4E1317` Schottky diode [?].

The `MA4E1317` has low total capacitance (.045 pF) and series resistance (4 Ω), minimizing parasitic losses. The datasheet also cites an operating frequency of up to 80 GHz for this diode, more than sufficient for our purposes. The forward voltage cited to be around .7 V, a typical value for most diodes [?]. A lower forward voltage would be desirable, and in considering future improvements to the system, this is definitely a point to consider.
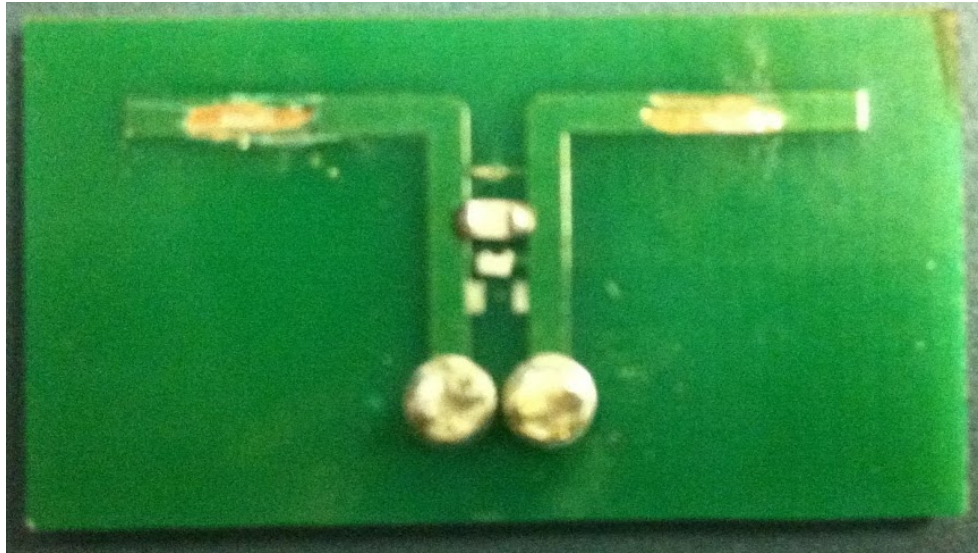
9.3   Antenna Design

A printed circuit board (PCB) dipole antenna was chosen for the system. The `MA4E1317` is a low-dimension flip-chip device, and is only suitable for mounting on a PCB. The design and specific parameters of the antenna is based off of the dual frequency WPT rectenna in [?], but has been modified heavily in our implementation. The design of the rectenna is shown in Figure 9-1.

The rectenna is composed of the `MA4E1317` diode, a 47 pF ceramic capacitor acting
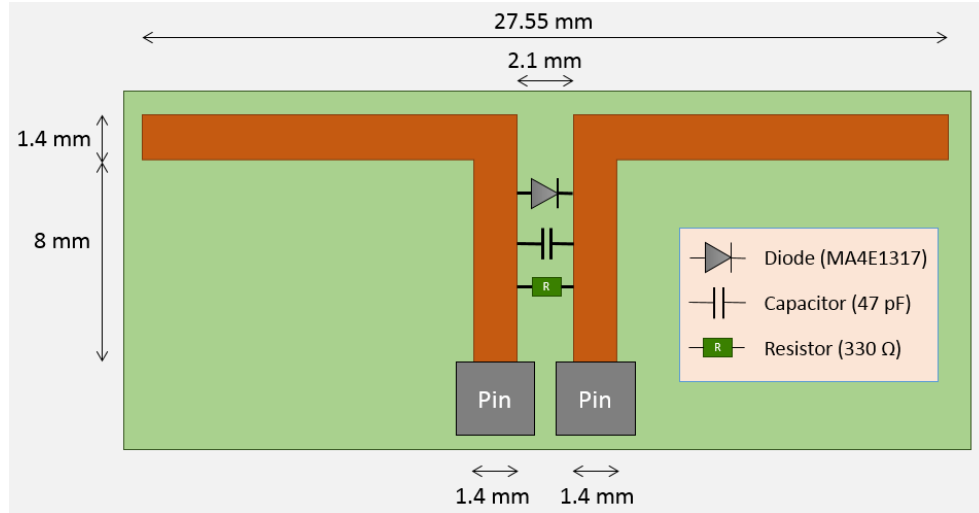
(a) A schematic of the PCB rectenna design and component specifications.

(b) Image of the assembled rectenna

Figure 9-1: Rectenna design

as a low-pass RF filter, a 330 Ω load resistor, and output pins for measurement purposes. The antenna is designed for operation at 5.45 GHz, so the length of the dipole is 27.55 mm, half the wavelength of the incident wave.

One important distinction for this rectenna design is the lack of filtering for higher-order harmonics. This feature is common in most rectennas, but is deliberately left out so that the antenna can generate nonlinear harmonics from the interrogation signal.

No special consideration for impedance matching between the antenna and the

rectifier components. This is definitely a point to consider for future improvement, as proper matching of the components should significantly improve the efficiency of rectification.

9.4   Rectenna Testing

To thoroughly test the rectenna, distinct tests were run to order to verify both its rectification and harmonic generation capabilities. We examined a range of frequencies for all tests to isolate peak performance.

9.4.1   DC Power Characterization

To determine the overall rectification efficiency, a second antenna was used to broadcast energy to the rectenna. A 17 dBm CW signal was generated from the PSG and broadcast through a monopole antenna. The rectenna was then positioned parallel to the broadcast antenna, at a distance of 2 cm. and the average DC voltage and power was measured over the load resistor. The test was repeated over a range of broadcast frequencies from 1 to 7 GHz. The setup is shown in Figure 9-2a and the results are shown in Figure 9-2b.

Rectification was most pronounced in the 3-5 GHz frequency band. Rectified voltage is highest at 3.4 GHz and 4.6 GHz, with DC voltage levels of 66.5 mV and 59.0 mV respectively. The transmission peak at 4.6 GHz is expected, given that in Figure 9-2b return loss is minimized at approximately 4.5 GHz. Unfortunately, DC voltage results of higher frequencies were unreliable and erratic given the measurement techniques, and accurate data could not be taken.

Given the resistive load of 330 Ω, rectified DC power can be calculated from the voltage above. A plot of this is shown in Figure 9-3.

Considering the input power of 17 dBm (around 50.12 mW), the wall-to-load efficiency of the experiment is extremely low for all frequencies. These losses can come from a number of sources, including bad coupling between the broadcast antenna and rectenna, reflection from broadcast antenna, losses in coaxial connections between
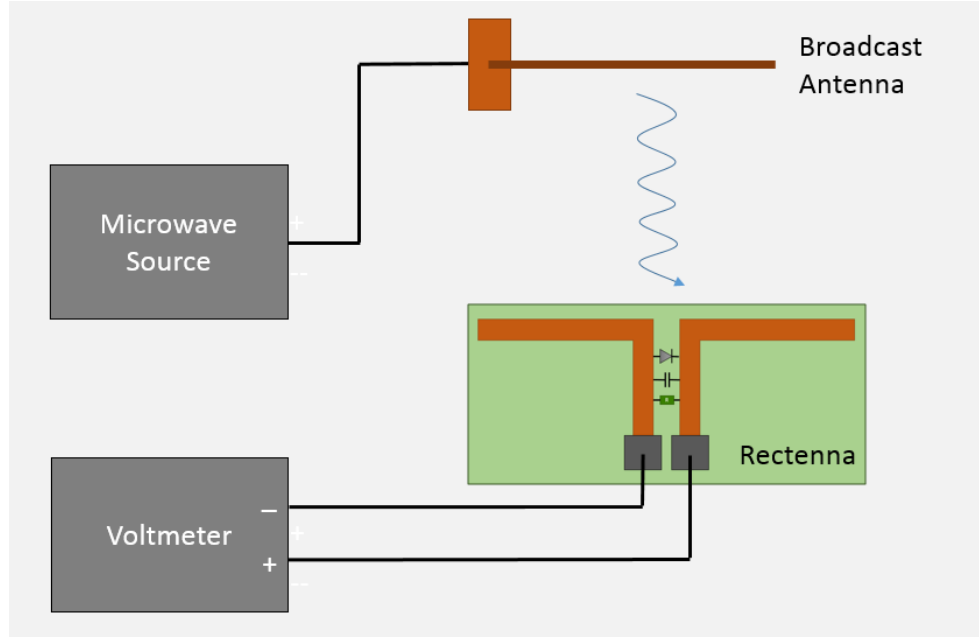
(a) Experimental setup for rectification testing
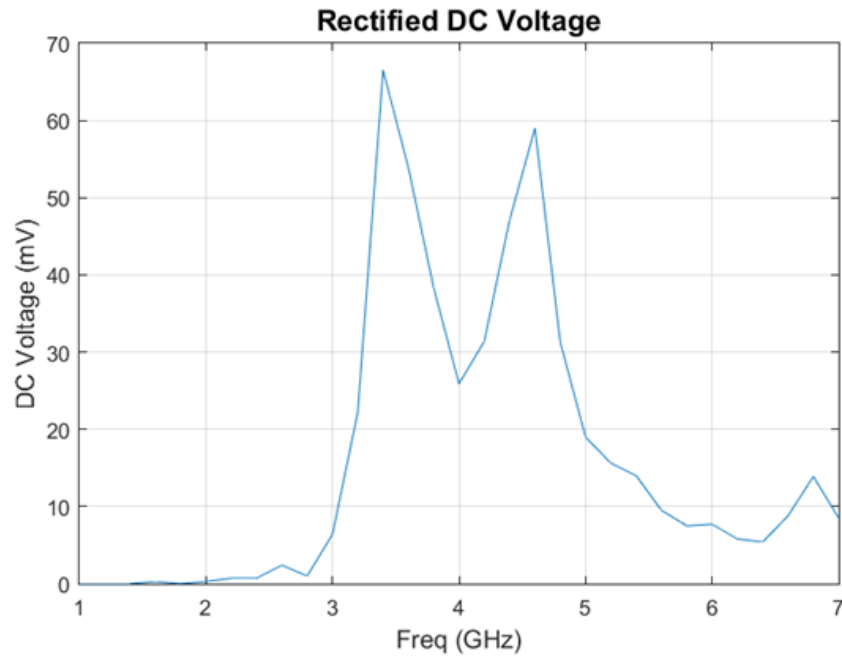
(b) DC voltage measured from the voltmeter in the setup on the left for a range (1-7 GHz) of frequency inputs.

components, and power radiated away from the rectenna, among others. However, the inherent losses of the experimental setup are not relevant to the overall efficiency of the system; for this, the efficiency result must be compared to only the rectification efficiency.
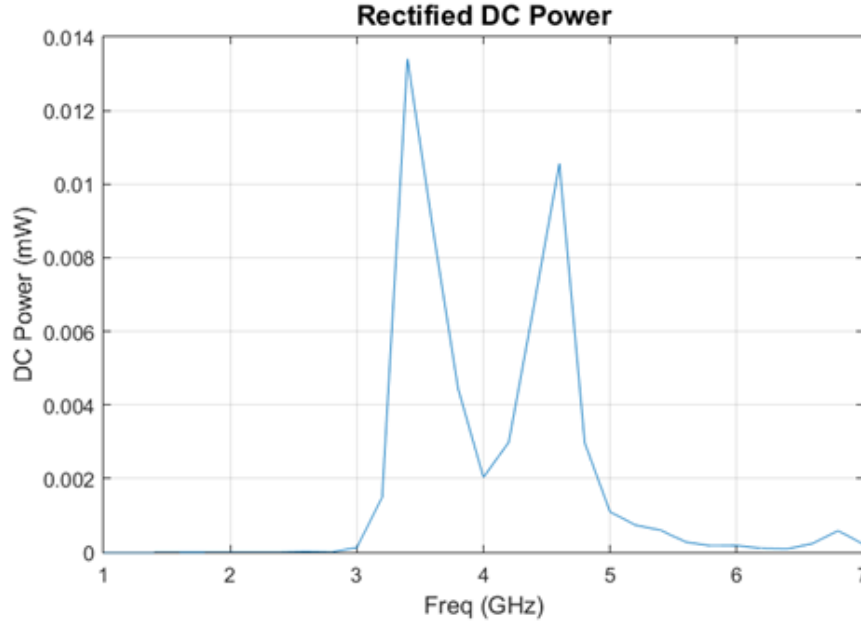
Figure 9-3: Rectified DC power calculated from DC voltage using the relation: $P = \frac{V^2}{R}$

To establish rectification efficiency, AC power tests were conducted on a bare dipole antenna with no diode, resistor, or capacitor. The results of this test establish the overall power accepted by the rectenna, and is directly comparable to the previous DC power results.

The setup of the AC power experiment was similar to the DC power experiment, with the exception of two key differences: the voltmeter was replaced by a DSO91304A oscilloscope, and the rectenna was replaced by the bare dipole antenna. In the absence of the 330 Ω load resistor on the rectenna, the 50 Ω input impedance of the oscilloscope [?] was used as the load. The setup and results of the test are shown below in Figures 9-4a and 9-4b, respectively.

Assuming that the transfer function between the antennas doesn't change between the AC and DC tests, these results allow the rectification efficiency to be calculated. The efficiency in this case is the ratio of the rectified DC power to the non-rectified AC power. Figure 9-5 shows the efficiency calculated this way, across the range of frequencies tested.

Analysis of the graph shows the same peak rectification efficiencies at 3.2 GHz
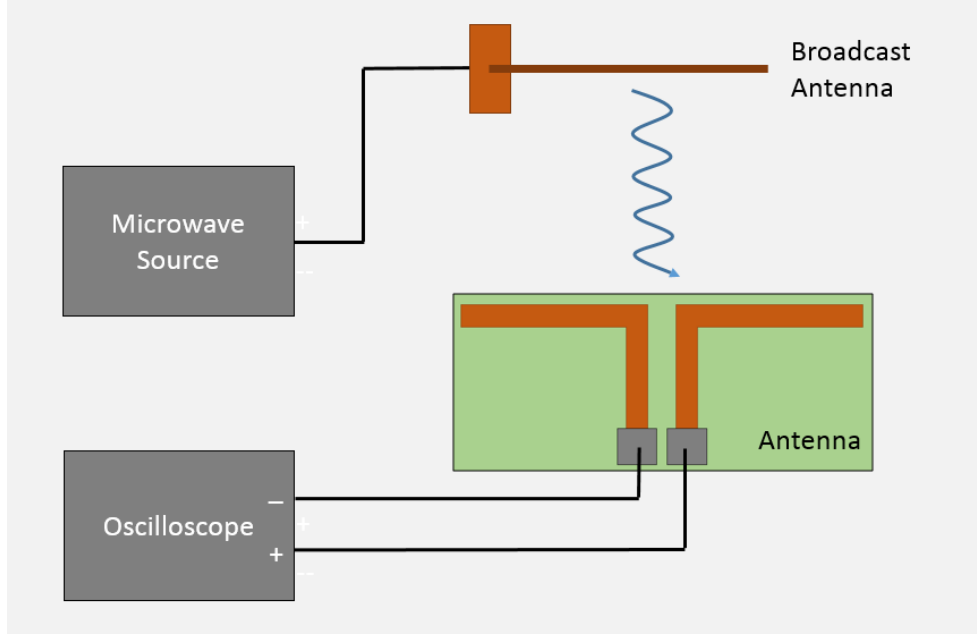
(a) Experimental setup for measuring accepted AC power
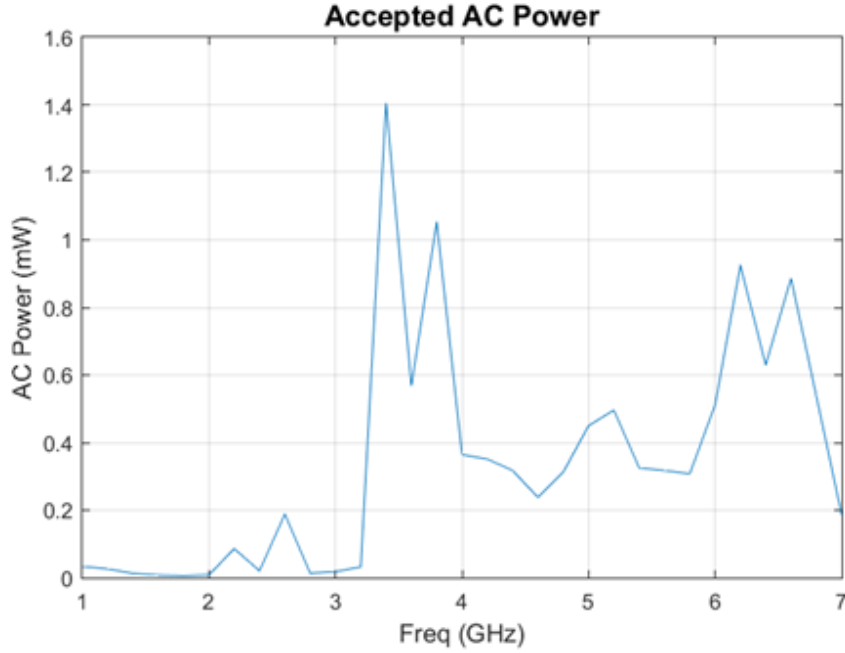
(b) Accepted AC power, used to establish a baseline for efficiency calculation, calculated using the relation $P = \frac{V_{max}^2}{2R}$.

and 4.6 GHz, with 4.7% and 4.4% respectively. This rather low efficiency is expected given the lack of optimization and impedance matching in the rectenna. However, this result clearly demonstrates rectification of high frequency AC power.
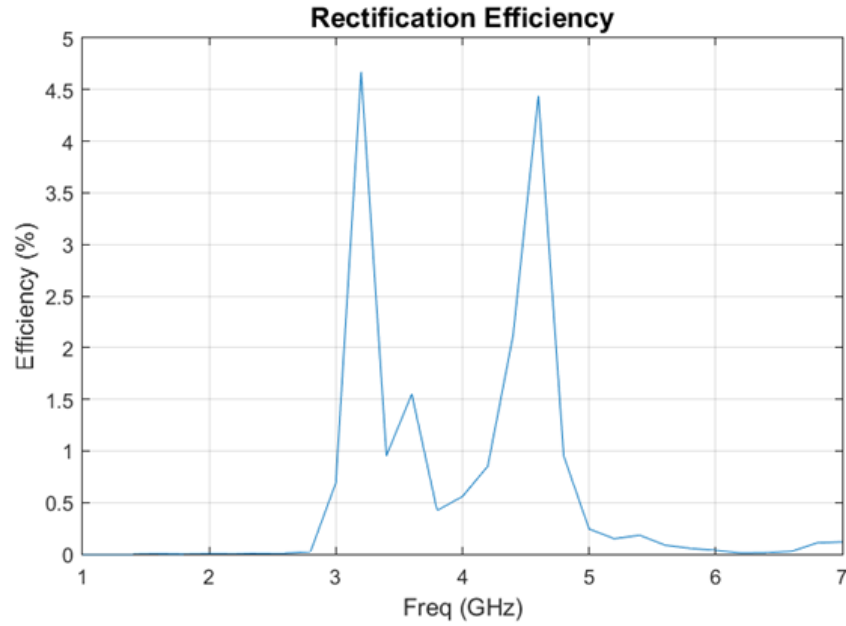
Figure 9-5: Rectification efficiency, calculated using accepted AC power as a baseline. Calculated using the ratio of rectified DC power to accepted AC power.

9.4.2 Harmonic Generation

Harmonic generation was then tested by measuring second harmonic power reflected from the rectenna. The antenna was stimulated by a 0 dBm CW signal, and the second harmonic reflected from the antenna was collected using a directional coupler feeding into the spectrum analyzer for measurement. The test setup for and results are shown in Figure 9-6.
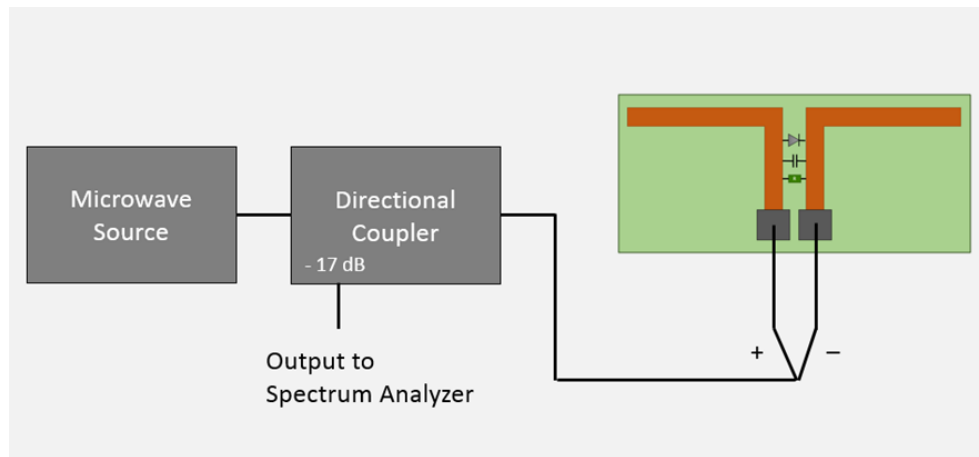

Figure 9-6: Experimental setup for harmonic generation testing.

In initial testing, the harmonic generation of the rectenna was minimal, as the measured 2nd harmonic power was comparable to the noise level power. However, after filtering out harmonic responses from microwave source, a distinct 2nd harmonic was found at 2.45 GHz at -150 dBm compared to the noise level power of -161 dBm. Bandwidth restrictions of filtering components prevented analysis of a full frequency spectrum, and thus, 2.45 GHz is the only frequency we were able to probe for harmonics. Even so, this result does demonstrate the harmonic generation capabilities of the rectenna.

9.5   Discussion

The intent of the rectenna was twofold. The rectenna was designed to rectify RF signals (1–10 GHz) and generate of higher-order harmonics. Both of these qualities are needed for the creation of an NLTR rectifier. The current experiments establish a baseline for rectification and harmonic generation that can be used for future designs.

The current design has made no steps towards the impedance matching of the antenna to the components. This is likely a major source of power lost by the system for rectification, and should be a top priority to consider in subsequent designs.

Our design of a dual-purpose rectenna satisfied our initial goals, and is a first step towards a functioning NLTR based WPT system. After considerable optimization and miniaturization, the rectenna would be used as a receiver for the electronics we want to power. After receiving the initial interrogation pulse and generating the 2nd harmonic response, it would then receive the main high power pulse and rectify the signal, providing the load device with DC power. Due to the nature of NLTR, the receiving devices donâĂŹt require power to facilitate the process.

Chapter 10

Conclusion

10.1 Future Work

TODO:...

10.2 Summary

TODO:...

Appendix A

Tables

Table A.1: Armadillos

Armadillos	are
our	friends

Appendix B

Figures

Figure B-1: Armadillo slaying lawyer.

Figure B-2: Armadillo eradicating national debt.

Bibliography

[1] First GSM-based communicator product hits the market Nokia Starts Sales of the Nokia 9000 Communicator, August 1996.

[2] A brief history of Wi-Fi. *The Economist*, June 2004.

[3] E. Barbieri and M. Meo. Time reversal DORT method applied to nonlinear elastic wave scattering. *Wave Motion*, 47(7):452–467, November 2010.

[4] Kenneth Butler. Tour WiTricityâĂŹs Room of Tomorrow: Wireless Charging ThatâĂŹs Flexible, December 2013.

[5] D. H. Chambers. Target characterization using time-reversal symmetry of wave propagation. *International Journal of Modern Physics B*, 21(20):3511–3555, August 2007.

[6] Matthew Frazier, Biniyam Taddese, Thomas Antonsen, and Steven M Anlage. Nonlinear time reversal in a wave chaotic system. *Physical review letters*, 110(6):063902, 2013.

[7] Matthew Frazier, Biniyam Taddese, Bo Xiao, Thomas Antonsen, Edward Ott, and Steven M Anlage. Nonlinear time reversal of classical waves: Experiment and model. *Physical Review E*, 88(6):062910, 2013.

[8] Eric Giler. A demo of Wireless Electricity, July 2009.

[9] Dennis H Goldstein and Edward Collett. *Polarized light.* Marcel Dekker, New York, 2003.

[10] Griffiths, David. *Introduction to Electrodynamics*. Prentice Hall, 3 edition, 1999.

[11] Sameer Hemmady, Xing Zheng, James Hart, Thomas M Antonsen Jr, Edward Ott, and Steven M Anlage. Universal properties of two-port scattering, impedance, and admittance matrices of wave-chaotic systems. *Physical Review E*, 74(3):036213, 2006.

[12] Sun K. Hong, Victor M. Mendez, Trystan Koch, Walter S. Wall, and Steven M. Anlage. Nonlinear Electromagnetic Time Reversal in an Open Semireverberant System. *Physical Review Applied*, 2(4), October 2014.

[13] Morris Kesler. Highly Resonant Wireless Power Transfer: Safe Efficient and over Distance. Technical report, WiTricity, Watertown MA, 2013.

[14] Dinh-Quy Nguyen and Woon-Seng Gan. The DORT solution in acoustic inverse scattering problem of a small elastic scatterer. *Ultrasonics*, 50(8):829–840, August 2010.

[15] C. Prada. The iterative time reversal mirror: A solution to self-focusing in the pulse echo mode. *The Journal of the Acoustical Society of America*, 90(2):1119, 1991.

[16] Claire Prada, SÃľbastien Manneville, Dimitri Spoliansky, and Mathias Fink. Decomposition of the time reversal operator: Detection and selective focusing on two scatterers. *The Journal of the Acoustical Society of America*, 99:2067, 1996.

[17] John B Schneider. Understanding the finite-difference time-domain method. *School of electrical engineering and computer science Washington State University.–URL: http://www. Eecs. Wsu. Edu/˜ schneidj/ufdtd/(request data: 29.11. 2012)*, 2010.

[18] David Hope Simpson, Chien Ting Chin, and Peter N. Burns. Pulse inversion Doppler: a new method for detecting nonlinear echoes from microbubble contrast agents. *Ultrasonics, Ferroelectrics, and Frequency Control, IEEE Transactions on*, 46(2):372–382, 1999.

[19] Walter Fox Smith. *Waves and oscillations: a prelude to quantum mechanics*. Oxford University Press, New York, 2010.

[20] Hans-JÃijrgen StÃűckmann. *Quantum Chaos: An Introduction*. Cambridge University Press, 2006.

[21] Biniyam Tesfaye Taddese, Thomas M. Antonsen, Edward Ott, and Steven M. Anlage. Sensing small changes in a wave chaotic scattering system. *Journal of Applied Physics*, 108(11):114911, 2010.

[22] Computer Simulation Technology. The finite integration technique. Retrieved fro mthe CST website https://www.cst.com/Products/CSTmws/FIT.

[23] N. Tesla. Apparatus for transmitting electrical energy. U.S. Patent, dec 1914. Patent US 1119732 A.

[24] C.A. Tucker, K. Warwick, and W. Holderbaum. A contribution to the wireless transmission of power. *International Journal of Electrical Power & Energy Systems*, 47:235–242, May 2013.

[25] M Clemens T Weiland. Discrete electromagnetism with the finite integration technique. *Progress In Electromagnetics Research*, 32:65–87, 2001.

[26] Huiqing Zhai, Helen K. Pan, and Mingyu Lu. A practical wireless charging system based on ultra-wideband retro-reflective beamforming. In *Antennas and Propagation Society International Symposium (APSURSI), 2010 IEEE*, pages 1–4, 2010.